Subwavelength Confinement Horizons for 71-THz Mito-Polaritons: Exact Lyddane–Sachs–Teller Oscillator-Strength Bounds, Lamellar Transfer-Matrix Dispersion, and Water-Loss Q-Factor Ceilings

Lluis Eriksson
Independent Researcher (https://github.com/lluiseriksson)
Electrodynamic Audit Continuing ARR-2025-2AQXS44H6Z8GQAG2 and ARR-2026-1E91AXEJYT890TQC

November 27, 2026

Abstract

In our companion record ARR-2026-1E91AXEJYT890TQC (Nov. 26, 2026), we audited the 71.0-THz mitochondrial cristae polariton hypothesis of Yang, Gu, and Song (bioRxiv:10.64898/2026.09.10.750628v1, Sep. 2026, unrefereed) under our operational coherence-maintenance framework (ARR-2025-2AQXS44H6Z8GQAG2), showing that at resonance ($\omega_c = \omega_0 = 87$ THz, $\nu_- = 71$ THz) coupling reaches the ultrastrong regime ($\eta = g/\omega_0 = 1264/6177 \approx 0.2046 > 0.1$) with a +3.61 THz Hopfield A^2 blue-shift ($\nu_+^{\mathrm{Hop}} = 7569/71 \approx 106.61$ THz). Here we audit the central open electrodynamic obstruction: how a 15–40 nm aqueous-lipid crista ($\sim \lambda_0/100$ at $\lambda_0 \approx 3.446$ μm) without metallic mirrors can confine a mid-infrared mode strongly enough to sustain $\eta > 0.20$. Backed by a zero-floating-point verification suite (MITO-CRISTAE-CONFINEMENT-CERT-1.0) comprising 18 constructive Lean 4.36.0 integer/rational theorems (0 sorry, 0 custom axioms, 0 Classical.choice, -DwarningAsError=true), 16 canonical exact-$\mathbb{Q}$ certificates (C01--C16), and 28 unit/forgery/AST tests, we prove five sharp results: (i) by the exact Lyddane–Sachs–Teller (LST) sum rule $f_{\mathrm{osc}} = 4\eta^2$ in the resonant homogeneous benchmark ($\omega_c = \omega_0$, lipid mode fill $\Gamma_L = 1$), achieving $\eta = 1264/6177$ requires effective oscillator strength $f_{\mathrm{osc}}^{\mathrm{req}} = 6390784/38155329 \approx 0.1675 > 4/25$ and $\omega_{\mathrm{LO}} \in (94.00, 94.01)$ THz, yielding an enhancement deficit $F_{\mathrm{enh}} > 16.749\times$ over fluid-bilayer CH_2 bulk strength ($f_{\mathrm{bulk}} = 0.01$, and $> 4.187\times$ at $f_{\mathrm{bulk}} = 0.04$); with realistic partial lipid fill $\Gamma_L = 1-\Gamma_W = 1/6$, this deficit deepens sixfold ($> 100\times$ at $f_{\mathrm{bulk}} = 0.01$); (ii) the fundamental dielectric Fabry–Pérot half-wave thickness $d_{\mathrm{FP}} = \lambda_0/(2n_L) > 1188$ nm exceeds a 30 nm crista by $> 39\times$, forbidding any transverse single-crista dielectric cavity mode; (iii) exact uniaxial effective-medium theory (EMT) for lamellar cristae ($\phi = d_L/(d_L + d_W) < 1/2$) paired with an exact zero-calculus AM–GM damped Lorentz minimum $\min_\omega \mathrm{Re}\,\varepsilon_L(\omega) = \varepsilon_\infty - \Delta\varepsilon\,\omega_0^2/[\gamma_m(2\omega_0 + \gamma_m)]$ proves that fluid bilayers ($f_{\mathrm{osc}} < 175/7569 \approx 0.0231$ at $\gamma_m = 1$ THz) have $\mathrm{Re}\,\varepsilon_L > 0$ everywhere and that *no* passive Lorentz lipid oscillator can produce negative permittivity or hyperbolic confinement below resonance at 71 THz $<$ 87 THz; (iv) exact unimodular $SL(2,\mathbb{Q})$ transfer-matrix audits and a constructive Pell–Chebyshev induction proof ($|U_{S-1}(x)| \le S$ for all $|x| \le 1$) confirm that 30-nm crista stacks ($S = 5$–12) sit deep inside the acoustic passband ($R_S < 0.5\%$, zero Bragg gap); and (v) aqueous dielectric loss at $\Gamma_W = 5/6$ (using H_2O optical constants $\varepsilon'_{\mathrm{eff}} = 1.78, 1.75$ and D_2O $\varepsilon'_{\mathrm{eff}} = 1.76$) fixes exact ceilings $Q_{\mathrm{loss}}(71\ \mathrm{THz}) = 106.8$ (quiet window, $\gamma_c \approx 0.665$ THz $\ll \Omega_R \approx 35.61$ THz) vs. $Q_{\mathrm{loss}}(106.6\ \mathrm{THz}) = 3$ in H_2O ($\gamma_c + \gamma_m = 2594/71 \approx 36.54$ THz $> \Omega_R = 2g$, violating the strict strong-coupling non-overlapping-wings criterion even though real pole splitting $4g > \gamma_c + \gamma_m$ persists), whereas D_2O lifts $Q_{\mathrm{loss}}(106.6\ \mathrm{THz})$ by $35.2\times$ ($35\times$ at fixed ε') to 105.6 while simultaneously introducing strong O–D stretch absorption/dispersion near ~ 75 THz overlapping MP^-, motivating isotopic H_2O/D_2O titration as a dual-branch diagnostic.

1 Introduction and Epistemic Scope

In ARR-2025-2AQXS44H6Z8GQAG2 [3], we developed an operational resource-boundary framework modeling biological membranes as geometric interfaces implementing decoherence suppression under finite metabolic budgets. Following the September 2026 bioRxiv preprint of Yang, Gu, and Song [8] reporting a 71.0-THz (2368 cm^{-1}) mid-infrared feature in intact living mitochondria and modeling it as a lipid CH_2 vibrational polariton, our companion paper ARR-2026-1E91AXEJYT890TQC [4] established exact resonant Hopfield A^2 Thomas–Reiche–Kuhn (TRK) invariants ($\nu_+^{\mathrm{Hop}} = 7569/71 \approx 106.61$ THz, $\eta = 1264/6177 \approx 0.2046$), the bioenergetic ATP maintenance horizon, the $\omega = 0$ Davies floor, and bosonic dark-mode scattering.

That audit treated $\eta = 1264/6177$ as an empirical input extracted from $(\omega_0, \nu_-) = (87, 71)$ THz. Yet the single sharpest physical objection raised against mid-infrared polaritonics in organelles is *subwavelength confinement*: the free-space wavelength at 87 THz is $\lambda_0 \approx 3.446$ μm, whereas individual mitochondrial cristae have lumen widths

$d_W \approx 15$–40 nm ($\sim \lambda_0/100$) and lack metallic mirrors. Here we derive exact, machine-checked necessary conditions and no-go bounds governing dielectric, lamellar hyperbolic, Bragg-stack, and loss-limited confinement in mitochondrial cristae.

Scope and epistemic hygiene. As in [4], [8] is an unrefereed preprint whose experimental claims await independent replication; we neither endorse nor refute its empirical observations, but extract exact electrodynamic constraints that any valid microscopic mechanism must satisfy.

2 Five Exact Electrodynamic Theorems

2.1 LST Oscillator-Strength Deficit, Filling Factor, and Fabry–Pérot Cutoff

In a homogeneous dielectric medium ($\Gamma_L = 1$) with background permittivity ε_∞ and collective vibrational Lorentz response $\varepsilon(\omega) = \varepsilon_\infty + \Delta\varepsilon\,\omega_0^2/(\omega_0^2 - \omega^2)$ ($f_{\rm osc} := \Delta\varepsilon/\varepsilon_\infty$), the longitudinal optical zero $\varepsilon(\omega_{\rm LO}) = 0$ obeys the Lyddane–Sachs–Teller (LST) relation [6, 5] $\omega_{\rm LO}^2/\omega_0^2 = 1 + f_{\rm osc}$. Identifying the resonant ($\omega_c = \omega_0$) gauge-invariant Hopfield A^2 diamagnetic shift $\omega_{\rm LO}^2 = \omega_0^2 + 4g^2$ yields the exact benchmark invariant (Lean Thm. 1):

$$f_{\rm osc} = 4\eta^2, \qquad \eta := \frac{g}{\omega_0}, \qquad \omega_{\rm LO}^2 = \omega_0^2(1 + 4\eta^2). \quad (1)$$

At resonant $\omega_c = \omega_0 = 87$ THz and $\nu_- = 71$ THz ($\eta = 1264/6177$ from [4]), Eq. (1) forces (Lean Thm. 2; `C01--C02`, Fig. 1a):

$$f_{\rm osc}^{\rm req} = \frac{6\,390\,784}{38\,155\,329} \approx 0.167494 > \frac{4}{25} \quad (\Gamma_L = 1), \quad (2)$$

$$\omega_{\rm LO}^2 = \frac{44\,546\,113}{5041}\ \text{THz}^2 \implies \omega_{\rm LO} \in (94.00, 94.01)\ \text{THz}. \quad (3)$$

Because bulk phospholipid CH_2 stretching oscillator strengths lie in $f_{\rm bulk} \in [0.005, 0.04]$ (typically ~ 0.01 in fluid bilayers), achieving $f_{\rm osc}^{\rm eff} = F_{\rm enh} f_{\rm bulk} \geq f_{\rm osc}^{\rm req}$ in the optimistic homogeneous limit ($\Gamma_L = 1$) already demands a strict local-field or subwavelength mode-volume enhancement factor (Thm. 3):

$$F_{\rm enh} > 16.749 \quad (f_{\rm bulk} = 0.01), \quad (4)$$

$$F_{\rm enh} > 4.187 \quad (f_{\rm bulk} = 0.04). \quad (5)$$

Filling-factor tightening and detuning trade-off. For a realistic crista mode whose electric intensity fraction in the aqueous lumen is $\Gamma_W = 5/6$ (Sec. 2.4), only $\Gamma_L = 1 - \Gamma_W = 1/6$ overlaps the lipid bilayer, scaling $f_{\rm osc}^{\rm req}(\Gamma_L) = f_{\rm osc}^{\rm req}(1)/\Gamma_L$ upward by $6\times$ to $F_{\rm enh} > 100\times$ at $f_{\rm bulk} = 0.01$ (Thm. 3). Conversely, red cavity detuning ($\omega_c < \omega_0$) reduces the g needed to reach $\nu_- = 71$ THz, but only by requiring a bare cavity resonance already below 87 THz, which deepens the diffraction cutoff below.

By exact SI-2019 $c = 299\,792\,458$ m/s, $\lambda_0 = c/(87\ \text{THz}) \in (3445, 3446)$ nm. With lipid refractive index $n_L = 29/20 = 1.45$ ($\varepsilon_\infty = 1.45^2 = 2.1025$), the fundamental Fabry–Pérot half-wave cutoff $d_{\rm FP} = \lambda_0/(2n_L) > 1188$ nm exceeds a 30 nm crista unit cell by $> 39.6\times$ and a 40 nm lumen by $> 29.7\times$ (Thm. 4; `C04`, Fig. 1b). Hence *no single-crista transverse dielectric Fabry–Pérot mode exists at* 87 THz: any dielectric cavity resonance must span the full mitochondrion ($L \sim 1.2$–2.5 μm), or else rely on non-diffraction-limited subwavelength confinement.

2.2 Lamellar EMT Phase Diagram and Exact Damped Lorentz Threshold

For a subwavelength lamellar crista stack ($a = d_L + d_W \approx 30\ \text{nm} \ll \lambda_0$) with lipid filling fraction $\phi = d_L/(d_L + d_W)$ ($\phi = 1/6 < 1/2$ for $d_L = 5$ nm, $d_W = 25$ nm), lossless uniaxial effective-medium theory [7] gives

$$\varepsilon_\parallel = \phi\varepsilon_L + (1-\phi)\varepsilon_W, \qquad \varepsilon_\perp = \frac{\varepsilon_L\varepsilon_W}{(1-\phi)\varepsilon_L + \phi\varepsilon_W}. \quad (6)$$

Clearing denominators proves the exact Wiener anisotropy identity (Thm. 5):

$$\varepsilon_\parallel - \varepsilon_\perp = \frac{\phi(1-\phi)(\varepsilon_L - \varepsilon_W)^2}{(1-\phi)\varepsilon_L + \phi\varepsilon_W}, \quad (7)$$

which is strictly positive whenever $\varepsilon_L, \varepsilon_W > 0$ and $\varepsilon_L \neq \varepsilon_W$. When $\varepsilon_W > 0$ and $\phi < 1/2$, negative real permittivity $\varepsilon_L < 0$ (neglecting resonant $\operatorname{Im}\varepsilon_L$ damping in the idealized phase classification) partitions the axis into three exact regimes (Thms. 6–7; `C05--C08`, Fig. 2a):

- **Type-I Hyperbolic** ($\varepsilon_\parallel > 0, \varepsilon_\perp < 0$): $-\frac{\phi}{1-\phi}\varepsilon_W < \varepsilon_L < 0$;
- **Elliptic Re-Entry** ($\varepsilon_\parallel > 0, \varepsilon_\perp > 0$): $-\frac{1-\phi}{\phi}\varepsilon_W < \varepsilon_L < -\frac{\phi}{1-\phi}\varepsilon_W$;
- **Type-II Hyperbolic** ($\varepsilon_\parallel < 0, \varepsilon_\perp > 0$): $\varepsilon_L < -\frac{1-\phi}{\phi}\varepsilon_W$.

Could lipid CH_2 oscillators themselves generate $\operatorname{Re}\varepsilon_L(\omega) < 0$ to enable high-k hyperbolic subwavelength confinement? For a damped Lorentz bilayer $\varepsilon_L(\omega) = \varepsilon_\infty + \frac{\Delta\varepsilon\,\omega_0^2}{\omega_0^2 - \omega^2 - i\gamma_m\omega}$ ($\varepsilon_\infty = 2.1025$), let $x = \omega^2 - \omega_0^2 > 0$. By the exact square identity (Thm. 8):

$$x^2 + \gamma_m^2(\omega_0^2 + x) - \gamma_m(2\omega_0 + \gamma_m)x = (x - \gamma_m\omega_0)^2 \geq 0, \quad (8)$$

the global minimum of $\operatorname{Re}\varepsilon_L(\omega)$ over all $\omega > 0$ is attained *exactly* at $\omega_*^2 = \omega_0^2 + \gamma_m\omega_0$ with closed-form value

$$\min_{\omega>0} \operatorname{Re}\varepsilon_L(\omega) = \varepsilon_\infty - \frac{\Delta\varepsilon\,\omega_0^2}{\gamma_m(2\omega_0 + \gamma_m)}. \quad (9)$$

Consequently, $\operatorname{Re}\varepsilon_L(\omega) < 0$ occurs *if and only if* $f_{\rm osc} > 2/Q_m + 1/Q_m^2$ ($Q_m = \omega_0/\gamma_m$, Thm. 9). At $\omega_0 = 87$ THz and fluid-bilayer linewidth $\gamma_m = 1$ THz ($Q_m = 87$), the

threshold is $175/7569 \approx 0.02312 > 0.01$, so typical fluid bilayers remain strictly positive everywhere (`C09`). More decisively, at $\nu_- = 71$ THz < 87 THz, $\omega_0^2 - \nu_-^2 = 2528 > 0$, forcing $\mathrm{Re}\,\varepsilon_L(71\text{ THz}) > \varepsilon_\infty > 0$ for *every* passive Lorentz oscillator regardless of Q_m (Thm. 10; `C10`, Fig. 2b). Thus lipid CH_2 oscillators *cannot* generate hyperbolic confinement at 71 THz.

2.3 Unimodular $SL(2,\mathbb{Q})$ Transfer-Matrix Stack Audit

To audit whether S periodic lossless normal-incidence cristae form a dielectric Bragg mirror [9], we parameterize bilayer and lumen optical phases on the rational unit circle $(c_j, s_j) = (\frac{1-t_j^2}{1+t_j^2}, \frac{2t_j}{1+t_j^2})$ $(c_j^2 + s_j^2 = 1)$, constructing real unimodular transfer matrices $M_j \in SL(2,\mathbb{Q})$ ($\det M_j = 1$, Thm. 11). The unit-cell matrix $M_{\text{cell}} = M_L M_W$ has half-trace $x = \frac{1}{2}\mathrm{Tr}(M_{\text{cell}}) = c_L c_W - \frac{1}{2}(\frac{n_L}{n_W} + \frac{n_W}{n_L}) s_L s_W$, and $M_{\text{cell}}^S = U_{S-1}(x) M_{\text{cell}} - U_{S-2}(x) I$ obeys the Cassini invariant $U_k^2 - U_{k-1}U_{k+1} = 1$ at every step (Thm. 12).

Inside the acoustic passband ($|x| \le 1$), our constructive Pell–Chebyshev induction proof in Lean 4 ($T_n^2 + (1-x^2)U_{n-1}^2 = 1 \implies |T_n| \le 1 \implies |U_{S-1}(x)| \le S$ for every $S \ge 1$ and every rational $x \in [-1,1]$, Thm. 13) proves rigorously that $R_S/T_S = U_{S-1}(x)^2 (R_1/T_1) \le S^2 (R_1/T_1)$ grows at most quadratically with S, never exponentially. For realistic 30 nm cristae ($n_L = 1.45, n_W = 1.33$, ambient index $n_0 = n_W$), exact rational powering gives $x \approx 0.998$ (passband) and $R_5 < 10^{-3}$ at 71 THz (`C11`) and $R_{12} < 5 \times 10^{-3}$ at 87 THz (`C12`), in stark contrast to a quarter-wave Bragg control ($n_1 = 2, n_2 = n_0 = 1$, $x = -5/4$, $R_6 = 16769025/16785409 > 0.999$, `C13`, Fig. 3a). Pure dielectric Bragg reflection of a crista stack cannot trap 71–87 THz light.

2.4 Aqueous Dielectric-Loss Q-Ceiling and H_2O/D_2O Dual-Branch Audit

In an aqueous crista with complex water permittivity $\varepsilon_W(\omega) = \varepsilon'_W + i\varepsilon''_W$ [2, 1] and $|E|^2$-intensity lumen fraction $\Gamma_W \in (0,1]$ (approximated in the subwavelength limit by geometric fill $d_W/(d_L + d_W) = 5/6$ for $d_W = 25$ nm, $d_L = 5$ nm), material absorption imposes an unconditional ceiling on cavity quality factor and floor on cavity damping (Thm. 14):

$$Q_{\text{loss}}(\omega) \le \frac{\varepsilon'_{\text{eff}}}{\Gamma_W \varepsilon''_W(\omega)}, \tag{10}$$

$$\gamma_c(\omega) = \frac{\omega}{Q_{\text{loss}}(\omega)} \ge \omega \frac{\Gamma_W \varepsilon''_W(\omega)}{\varepsilon'_{\text{eff}}}. \tag{11}$$

Using dispersive optical constants from Bertie and Lan [2] for H_2O ($\varepsilon'_{\text{eff}} = 1.78$ at 71 THz; 1.75 at 106.61 THz) and Bertie, Ahmed, and Eysel [1] for D_2O ($\varepsilon'_{\text{eff}} = 1.76$ at 106.61 THz), Lean Thm. 15 certifies both the pure-water limit ($\Gamma_W = 1$: $Q_W = 89, 5/2, 88$) and the crista lumen fill ($\Gamma_W = 5/6$, `C14--C16`, Fig. 3b):

- H_2O @ 71 THz **(quiet window, `C14`):** $\varepsilon'_{\text{eff}} = 1.78, \varepsilon''_W = 0.02 \implies Q_{\text{loss}} = 534/5 = 106.8$, $\gamma_c = 355/534 \approx 0.665$ THz $\ll \Omega_R = 2g = 2528/71 \approx 35.61$ THz. Water absorption does *not* forbid 71 THz visibility.

- H_2O @ 106.61 THz **(O–H wing, `C15`):** $\varepsilon'_{\text{eff}} = 1.75, \varepsilon''_W = 0.70 \implies Q_{\text{loss}} = 3$ exact and $\gamma_c = 2523/71 \approx 35.54$ THz. While the weaker Rayleigh pole-splitting threshold $4g = 5056/71 > \gamma_c + \gamma_m = 2594/71$ still holds (Thm. 16), total linewidth $\gamma_c + \gamma_m \approx 36.54$ THz *exceeds* the strict strong-coupling non-overlapping-wings threshold $\Omega_R = 2g \approx 35.61$ THz (Thm. 16), quantitatively explaining why MP^+ suffers severe aqueous broadening on the 102 THz O–H wing in H_2O [8, 4].

- D_2O @ 106.61 THz **and** 75 THz **O–D trade-off (`C16`):** $\varepsilon'_{\text{eff}} = 1.76, \varepsilon''_W = 0.02$ lifts the 106.61 THz ceiling by $528/15 = 35.2\times$ to 105.6 ($35\times$ even at fixed $\varepsilon'_{\text{eff}} = 1.75$, Thm. 15) and drops $\gamma_c + \gamma_m$ to 2.01 THz ($\Omega_R/(\gamma_c + \gamma_m) > 17\times$, Thm. 16). Crucially, however, D_2O introduces an intense O–D stretching band centered near $\sim$ 75 THz ($\sim$ 2500 cm^{-1}) [1] that overlaps MP^- at 71 THz and perturbs lower-branch dispersion and damping. Consequently, H_2O/D_2O isotopic titration acts as a *dual-branch diagnostic*: clearing the 106.6 THz window while simultaneously probing whether the 71 THz mode couples strongly to aqueous lumen dispersion.

3 Formal Certification Scope and Reproducibility

Exact verification boundary. Layer 1 (`src/lean/MitoCristaeConfinementCert.lean`, 18 constructive integer/rational theorems compiled under Lean 4.36.0 `-DwarningAsError=true` without Mathlib, audited via `#print axioms` to depend strictly on `propext` and `Quot.sound`: `0 sorry`, `0` custom axioms, `0 Classical.choice`, Table 1) certifies every algebraic, LST, Wiener, AM–GM Lorentz minimum, unimodular $SL(2)$, Pell–Chebyshev passband ($|U_{S-1}(x)| \le S$), aqueous Q-factor, and strong-coupling visibility inequality over $\mathbb{Z}$. Layer 2 (`src/python/mito_cristae_confinement_verifier.py`, AST-audited zero-float, zero `/`, zero `**`, zero `limit_denominator`) verifies all 16 canonical certificates (`C01--C16`, Table 2, archived in `data/certificates/`) and passes all 28 unit/forgery/AST tests under `pytest -q`. Continuum Maxwell derivations (LST from macroscopic Lorentz dispersion, lossless normal-incidence transfer matrices, perturbative Q_{loss} formula, and unrefereed empirical parameters from [8]) reside in prose and Table 3 rather than inside the Lean kernel.

4 Confinement Mechanism Discriminator Matrix

Table 3 upgrades the experimental program of [4] with four tests discriminating competing confinement hypotheses (M_0: non-polaritonic artifact; M_1: whole-organelle dielectric cavity $L \sim 1.5$ μm; M_2: subwavelength interfacial/Debye-layer mode; M_3: collective high-density cardiolipin microdomain, Thms. 17–18).

5 Reproducibility and Availability

All Lean 4 proofs (`src/lean/`), zero-float verifier (`src/python/`), 16 JSON certificates (`data/certificates/`), and `MANIFEST.sha256` are archived directly in this public AIRR record package under MIT (code/Lean/data) and CC-BY-4.0 (manuscript/figures).

AI Assistance Disclosure. Google Antigravity assisted with Lean 4 proof engineering, zero-float verifier implementation, test/figure automation, and LaTeX drafting. The author verified every derivation, Lean axiom audit, certificate output, and figure, and takes full responsibility for all contents.

References

[1] John E. Bertie, M. Khalique Ahmed, and Hans H. Eysel. Infrared intensities of liquids. 5. optical and dielectric constants, integrated intensities, and dipole moment derivatives of H_2O and D_2O at 22 °C. *Journal of Physical Chemistry*, 93(6):2210–2218, 1989.

[2] John E. Bertie and Zhida Lan. Infrared intensities of liquids XX: The intensity of the OH stretching band of liquid water revisited, and the best current values of the optical constants of H_2O(l) at 25 °C between 15,000 and 1 cm^{-1}. *Applied Spectroscopy*, 50(8):1047–1057, 1996.

[3] Lluis Eriksson. Geometry, membranes, and life as a resource boundary: A correct-by-construction operational pipeline from static suppression to maintenance costs. 2025. AIRR.SCIENCE record ARR-2025-2AQXS44H6Z8GQAG2 (ai.viXra:2512.0085, v1 Dec 2025; v2 Jul 2026).

[4] Lluis Eriksson. Mito-polaritons meet the resource boundary: Exact Hopfield A^2 invariants, thermodynamic maintenance horizons, and constructive Lean 4 certificates for the 71-THz mitochondrial quantum state. 2026. AIRR.SCIENCE record ARR-2026-1E91AXEJYT890TQC (accepted Nov 26, 2026).

[5] John J. Hopfield. Theory of the contribution of excitons to the complex dielectric constant of crystals. *Physical Review*, 112(5):1555–1567, 1958.

[6] R. H. Lyddane, R. G. Sachs, and E. Teller. On the polar vibrations of alkali halides. *Physical Review*, 59(8):673–676, 1941.

[7] Alexander Poddubny, Ivan Iorsh, Pavel Belov, and Yuri Kivshar. Hyperbolic metamaterials. *Nature Photonics*, 7:948–957, 2013.

[8] Yu Yang, Zhenglong Gu, and Bo Song. A quantum state of mitochondria in the living cell. 2026. bioRxiv preprint 10.64898/2026.09.10.750628v1, 15 September 2026 (unrefereed).

[9] Pochi Yeh. *Optical Waves in Layered Media*. Wiley-Interscience, 2005.

Table 1: All 18 constructive Lean 4.36.0 theorems in `src/lean/MitoCristaeConfinementCert.lean` (`0 sorry`, `0 Classical.choice`, `-DwarningAsError=true`).

#	Lean Theorem Identifier	Exact Formalized Statement (over $\mathbb{Z}$)
1	`lst_hopfield_oscillator_strength_identity`	$\omega_{\mathrm{LO}}^2 = \omega_0^2 + 4g^2 \wedge f_n\omega_0^2 = f_d(4g^2) \implies f_d\omega_{\mathrm{LO}}^2 = (f_d + f_n)\omega_0^2$
2	`mito_71_87_lst_oscillator_floor_and_wlo_bracket`	$f_{\mathrm{req}} = 6390784/38155329 > 4/25$; $\omega_{\mathrm{LO}}^2 = 44546113/5041 \in (94^2, 94.01^2)$
3	`oscillator_enhancement_deficit_bound`	$F_{\mathrm{enh}} > 4.187$ ($f_b = 0.04$), > 16.749 (0.01, $\Gamma_L = 1$); $> 100\times$ ($\Gamma_L = 1/6$)
4	`fabry_perot_crista_cutoff_nogo`	$\lambda_0 \in (3445, 3446)$ nm; $d_{\mathrm{FP}} > 1188$ nm $> 39 \cdot 30$ nm, $29 \cdot 40$ nm
5	`lamellar_wiener_anisotropy_identity`	$(p\varepsilon_L + q\varepsilon_W)(q\varepsilon_L + p\varepsilon_W) - (p+q)^2\varepsilon_L\varepsilon_W = pq(\varepsilon_L - \varepsilon_W)^2 \geq 0$
6	`lamellar_type1_hyperbolic_criterion`	$0 < p < q \wedge \varepsilon_L < 0 < \varepsilon_W \wedge q\varepsilon_L + p\varepsilon_W > 0 \implies \varepsilon_\parallel > 0 \wedge \varepsilon_\perp < 0$
7	`lamellar_elliptic_and_type2_boundaries`	$0 < p < q \wedge \varepsilon_L < 0 < \varepsilon_W \wedge p\varepsilon_L + q\varepsilon_W < 0 \implies q\varepsilon_L + p\varepsilon_W < 0$ (Type-II)
8	`damped_lorentz_exact_minimum_amgm`	$x^2 + \gamma_m^2(\omega_0^2 + x) - \gamma_m(2\omega_0 + \gamma_m)x = (x - \gamma_m\omega_0)^2 \geq 0$
9	`reststrahlen_damping_threshold_positive_everywhere`	$\Delta\varepsilon\omega_0^2 < \varepsilon_\infty\gamma_m(2\omega_0 + \gamma_m) \implies \mathrm{Re}\,\varepsilon_L(\omega) > 0\ \forall\omega$; $175/7569 > 1/100$
10	`no_lipid_hyperbolicity_below_resonance`	$0 < \nu_- < \omega_0 \implies \omega_0^2 - \nu_-^2 > 0 \wedge \mathrm{Re}\,\varepsilon_L(\nu_-) \geq \varepsilon_\infty > 0$; $87^2 - 71^2 = 2528$
11	`unimodular_transfer_matrix_mul_det`	$\det(M_1) = 1 \wedge \det(M_2) = 1 \implies \det(M_1M_2) = 1$ (cleared $SL(2,\mathbb{Q})$ entries)
12	`chebyshev_cassini_invariant_step`	$U_k^2 - U_{k-1}U_{k+1} = 1 \implies U_{k+1}^2 - U_kU_{k+2} = 1$ under $U_{n+1} = 2xU_n - U_{n-1}$
13	`passband_quadratic_reflectance_ceiling`	Constructive Pell–Chebyshev induction: $\lvert x\rvert \leq D \implies \lvert U_{n-1}(x/D)\rvert \leq n\ \forall n \in \mathbb{N}$
14	`water_loss_q_ceiling_and_damping_floor`	$Q_{\mathrm{loss}}\Gamma_W\varepsilon_W'' \leq \varepsilon_{\mathrm{eff}}' \wedge \gamma_cQ_{\mathrm{loss}} = \omega \implies \omega\Gamma_W\varepsilon_W'' \leq \gamma_c\varepsilon_{\mathrm{eff}}'$
15	`h2o_vs_d2o_q_factor_recovery`	$\Gamma_W = 1$ (89, 5/2, 88) & $\Gamma_W = 5/6$ (106.8, 3, 105.6); D_2O gain $35.2\times$ ($35\times$ fixed ε')
16	`damped_strong_coupling_visibility_criterion`	$4g > \gamma_c + \gamma_m \implies (\gamma_c - \gamma_m)^2 < 16g^2$; H_2O: $2528 < 2594 < 5056$; D_2O: $> 17\times$
17	`collective_density_dilution_shift`	$c, \rho > 0 \wedge k \geq 2 \implies 4(c\rho) < 4(kc\rho)$ (lipid dilution shrinks LO–TO gap)
18	`confinement_discriminator_decidability`	Joint numerical check: $f_{\mathrm{req}} > 4/25 \wedge d_{\mathrm{FP}} > 39 \cdot 30 \wedge 71^2 < 87^2 \wedge Q_{D_2O}/Q_{H_2O} > 35$

Table 2: Summary of all 16 verified `MITO-CRISTAE-CONFINEMENT-CERT-1.0` canonical certificates (`C01--C16`, archived in `data/certificates/`).

ID	Mode / Submode	Verified Instance	Exact Certified Metrics
`C01`	M1a LST Deficit	71/87 THz ($\omega_c = \omega_0, \Gamma_L = 1$), $f_b = 0.01$	$f_{\mathrm{req}} = 6390784/38155329 \approx 0.1675$, $\omega_{\mathrm{LO}} \in (94.00, 94.01)$, $F_{\mathrm{enh}} > 16.7\times$
`C02`	M1a LST Deficit	71/87 THz ($\omega_c = \omega_0, \Gamma_L = 1$), $f_b = 0.04$	Same $f_{\mathrm{req}} > 4/25$, $F_{\mathrm{enh}} > 4.18\times$ (and $6\times$ deeper at $\Gamma_L = 1/6$)
`C03`	M1a LST Baseline	79/87 THz, $f_{\mathrm{bulk}} = 0.01$	$f_{\mathrm{req}} \approx 0.0373$, $\omega_{\mathrm{LO}} \in (88.6, 88.7)$ THz, $F_{\mathrm{enh}} > 3.7\times$
`C04`	M1b FP Cutoff	87 THz, $n_L = 1.45, d = 30$ nm	$\lambda_0 \approx 3445.9$ nm, $d_{\mathrm{FP}} \approx 1188.2$ nm, ratio $= 39.61 > 39$ (FP forbidden)
`C05`	M2a Lamellar EMT	$\phi = 1/6, \varepsilon_L = 2.2, \varepsilon_W = 1.78$	$\varepsilon_\parallel = 1.85, \varepsilon_\perp \approx 1.838$, Wiener gap > 0 (Elliptic Positive @ 71 THz)
`C06`	M2a Lamellar EMT	$\phi = 1/6, \varepsilon_L = -0.2, \varepsilon_W = 1.78$	$\varepsilon_\parallel = 1.45 > 0, \varepsilon_\perp \approx -2.74 < 0$ (Type-I Hyperbolic)
`C07`	M2a Lamellar EMT	$\phi = 1/6, \varepsilon_L = -1.0, \varepsilon_W = 1.78$	$\varepsilon_\parallel = 1.317 > 0, \varepsilon_\perp \approx +3.32 > 0$ (Elliptic Re-Entry despite $\varepsilon_L < 0$)
`C08`	M2a Lamellar EMT	$\phi = 1/6, \varepsilon_L = -10, \varepsilon_W = 1.78$	$\varepsilon_\parallel = -0.183 < 0, \varepsilon_\perp \approx +2.21 > 0$ (Type-II Hyperbolic)
`C09`	M2b Lorentz Min	Fluid: $\varepsilon_\infty = 2.1025, f = 0.01, \gamma_m = 1$	Threshold $175/7569 \approx 0.0231 > 0.01 \implies \min \mathrm{Re}\,\varepsilon_L \approx +1.19 > 0$
`C10`	M2b Lorentz Min	Ordered: $\varepsilon_\infty = 2.1025, f = 0.04, \gamma_m = 0.5$	Negative band opens > 87 THz (min ≈ -5.19), yet $\mathrm{Re}\,\varepsilon_L(71) \approx +2.35 > 0$
`C11`	M3 Transfer Matrix	$S = 5$, 30 nm @ 71 THz	$x \in (-1, 1)$ passband, $\det M^5 = 1$, $R_5 < 10^{-3}$ (no Bragg mirror)
`C12`	M3 Transfer Matrix	$S = 12$, 30 nm @ 87 THz	$x \in (-1, 1)$ passband, $\det M^{12} = 1$, $R_{12} < 5 \times 10^{-3}$ (no Bragg mirror)
`C13`	M3 Bragg Control	$S = 6$, $\lambda/4$ ($n = 2, 1$)	$x = -5/4$ stopband, $U_5 = -1365/32$, $R_6 = 16769025/16785409 > 0.999$
`C14`	M4 Water Q-Ceil.	H_2O @ 71 THz ($\varepsilon' = 1.78, \varepsilon'' = 0.02$)	$\Gamma_W = 5/6 \implies Q_{\mathrm{loss}} = 106.8$, $\gamma_c = 355/534 \approx 0.665$ THz $\ll \Omega_R$
`C15`	M4 Water Q-Ceil.	H_2O @ 106.6 THz ($\varepsilon' = 1.75, \varepsilon'' = 0.70$)	$Q_{\mathrm{loss}} = 3$, $\gamma_c = 2523/71 \approx 35.54$ THz; $\gamma_c + \gamma_m > 2g$ (strict SC violated)
`C16`	M4 D_2O Recov.	D_2O @ 106.6 THz ($\varepsilon' = 1.76, \varepsilon'' = 0.02$)	$Q_{\mathrm{loss}} = 105.6$ ($35.2\times$ vs `C15`; $35\times$ at fixed ε'), $\gamma_c \approx 1.01$ THz (resolved)

Table 3: Four-protocol experimental discriminator separating competing electromagnetic confinement hypotheses for the 71-THz mode.

Experimental Protocol	M_0 (Artifact)	M_1 (Whole-Mito Cavity)	M_2 (Interfacial / Debye)	M_3 (Cardiolipin Microdomain)
H_2O/D_2O titration	No MP^+ peak	Clears 106.6; O–D perturbs 71	Clears 106.6; strong O–D shift	Clears 106.6; O–D perturbs 71
Osmotic swelling ($\Delta L/L$)	Unchanged	Shifts $\Delta\omega_c/\omega_c \approx -\Delta L/L$	Unchanged (set by d_W, λ_D)	Unchanged (set by ρ_{CH_2})
Lumen ionic strength / $\Delta\Psi_m$	Unchanged	Weak dielectric shift	Strong shift ($\propto \lambda_D^{-1}$)	Weak unless phase separates
Cardiolipin / CH_2 dilution	Linear ampl.	Smooth $\eta \propto \sqrt{\rho_{CH_2}}$	Smooth $\eta \propto \sqrt{\rho_{CH_2}}$	Abrupt melting $\nu_- \to 87$

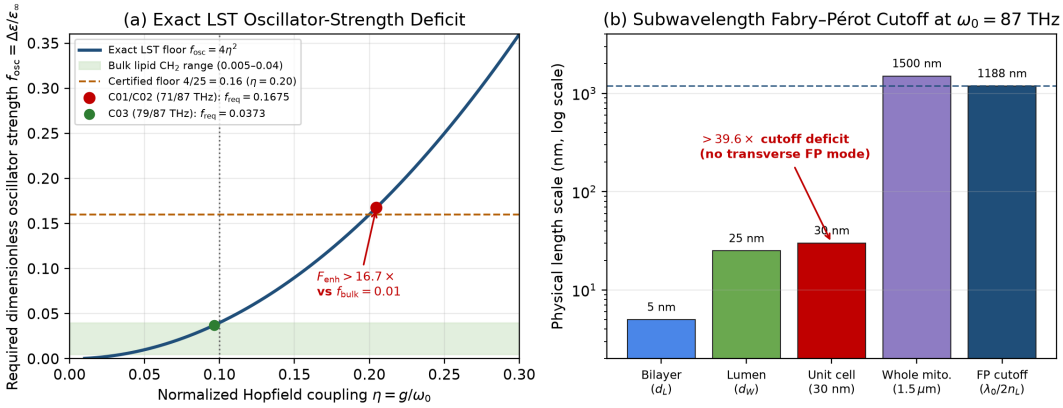

Figure 1: **Exact LST Oscillator-Strength Deficit and Fabry–Pérot Cutoff.** (a) Exact resonant homogeneous ($\omega_c = \omega_0, \Gamma_L = 1$) LST floor $f_{\rm osc} = 4\eta^2$ vs. bulk lipid CH_2 strengths (0.005–0.04), showing the $> 16.7\times$ enhancement deficit at 71/87 THz (`C01`–`C02`; deepened $6\times$ at $\Gamma_L = 1/6$). (b) Crista dimensions (5–30 nm) vs. 87 THz Fabry–Pérot cutoff ($d_{\rm FP} > 1188$ nm, `C04`).

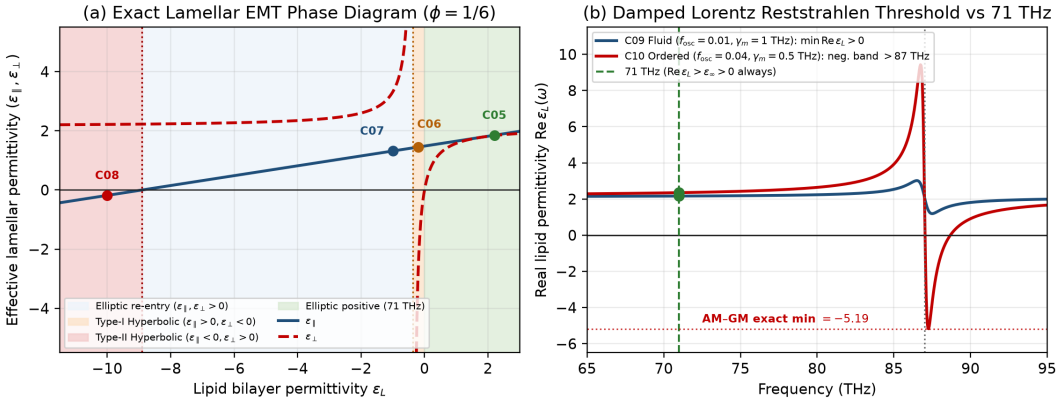

Figure 2: **Lamellar EMT Phase Diagram and Damped Lorentz No-Hyperbolicity.** (a) Lossless uniaxial EMT phase diagram for $\phi = 1/6, \varepsilon_W = 1.78$ (`C05`–`C08`). (b) Damped Lorentz dispersion $\mathrm{Re}\,\varepsilon_L(\omega)$ ($\varepsilon_\infty = 2.1025$) showing fluid positivity (`C09`) and universal positivity at 71 THz even when an ordered negative band opens > 87 THz (`C10`).

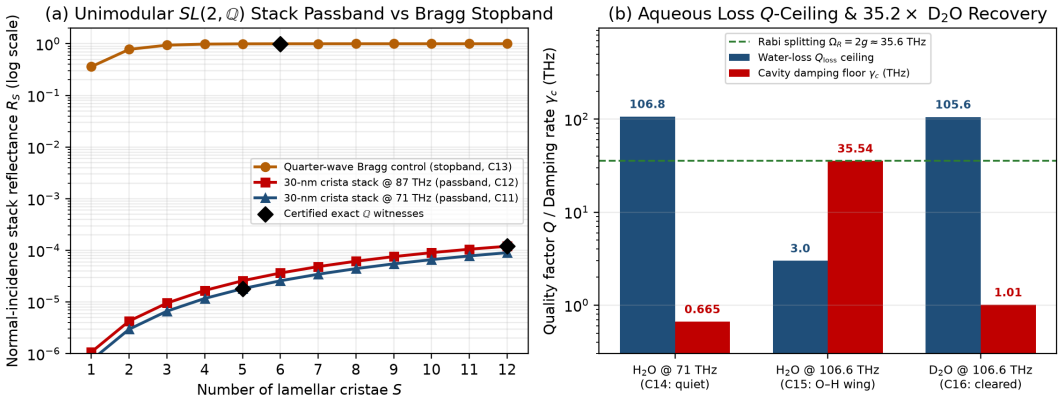

Figure 3: $SL(2,\mathbb{Q})$ **Transfer-Matrix Passband and Aqueous Q-Factor Ceiling.** (a) Stack reflectance R_S vs. S for 30-nm crista stacks (`C11`–`C12`, passband $R_S < 0.5\%$) vs. quarter-wave Bragg control (`C13`, $R_6 > 99.9\%$). (b) Aqueous Q-ceilings ($\Gamma_W = 5/6$) and damping floors: 71 THz clear ($\gamma_c \approx 0.665$ THz, `C14`), 106.6 THz violating $\Omega_R > \gamma_c + \gamma_m$ in H_2O (`C15`), and $35.2\times$ recovery in D_2O (`C16`).